DOI: 10.1002/ejic.200900536

Coordination Induction of Nonlinear Molecular Shape in Mesomorphic and Luminescent Zn^{II} Complexes Based on Salen-Like Frameworks

Daniela Pucci,*[a] Iolinda Aiello,[a] Anna Bellusci,[a] Alessandra Crispini,[b] Mauro Ghedini,[a] and Massimo La Deda[b]

Keywords: Zinc / Schiff bases / Metallomesogens / Nonlinear shape / Intercalated smectic phase

A series of tetradentate dimeric salicylaldimine ligands ($H_2L_nR_m$) with terminal chains of variable length (R_m) and a central flexible $(CH_2)_n$ spacer (L_n = 10 and 12) was synthesized. For all ligands, according to their rod-like molecular shape, mesomorphism characteristic of calamitic systems (nematic and smectic C phases) is observed. The reaction with Zn^{II} acetate dihydrate afforded a series of ZnL_nR_m derivatives (**1**–**6**) that show mesomorphic behaviour only in the presence of the longest terminal tails (R_{12}). Interestingly, the flexibility of the very long spacer in the central core and the presence of the tetrahedral Zn^{II} centre introduce nonlinearity in the central part of the molecule, responsible for the appearance of an intercalated smectic C mesophase. Moreover, the coordination of the Zn^{II} ion to the salen-like framework induces, in all the corresponding complexes, interesting blue-light-emitting properties at room temperature in dichloromethane solution (EQY in the 19–22% range at about 450 nm), as well as in the solid (EQY: 9% at about 450 nm) or, when present, in the mesophase (EQY 8% at 440 nm).

Introduction

Zn^{II} complexes displaying physical properties such as thermal stability, luminescence in the visible region of the electromagnetic spectrum and/or charge transporting ability are very attractive species for applications in electroptic devices.[1] The different practical applications involving molecular materials processed as amorphous thin films imply the use of technological approaches able to obtain useful thin layers such as high-vacuum evaporation or solutions, the latter way being less expensive and more suitable for large area devices. In this context, the synthesis of Zn^{II} compounds featuring good solubility in appropriate solvents is required. However, the performances of these devices are also strongly dependent on the efficiency of the charge transport and the emission, both properties ultimately depending on the molecular arrangement inside the amorphous films. Therefore, in order to optimize properly the devices, the development of new soft materials such as liquid crystals, showing at the same time order and charge mobility, seems to be a good strategy.[2] Indeed, in the last years it has been proven that the opportune combination of nonconventional shapes and supramolecular assemblies allowed the first examples of mesomorphic Zn^{II} species showing lamellar or columnar liquid crystalline phases to be obtained.[3]

In particular, Zn^{II} complexes based on versatile salen (*N*,*N*′-bis-salicylidene ethylenediamine) frameworks are receiving growing interest as cheap and accessible building blocks for the synthesis of new molecular materials working as the light-emitting layer in OLEDs (organic light-emitting devices).[4]

In a recent paper we reported on the excellent emission quantum yield displayed by the blue-emitting chromophore obtained through Zn^{II} complexation with the salen-like ligand H_2L_{12} containing a very long, central alkyl backbone (Scheme 1).[5] From this study it appears evident that the emission performances are strongly related to the nature of the bridging diamine and therefore to the molecular structure of the resulting coordination compound.

In order to combine the emissive properties of these systems with the development of softness through mesomorphic induction, promesogenic building blocks have been introduced[6] as alkoxy substituents in the 4-position of the aromatic rings connected to the salicylaldimine moiety through an ester link ($H_2L_{12}R_m$ in Scheme 1) in analogy with reference ligands containing shorter central bridges.[7] Our first attempts to obtain metal-containing salen-like liquid crystals by using these new ligands involved the use of Ni^{II} and Cu^{II} metal ions. Interestingly, such M^{II} complexation afforded 1:1 metal-to-ligand compounds (with a square planar M^{II} coordination geometry, regular for Ni^{II}

[a] Centro di Eccellenza CEMIF.CAL, LASCAMM - CR INSTM, Unità INSTM della Calabria and LiCryl, CNR-INFM, Dipartimento di Chimica - Università della Calabria, 87036 Arcavacata di Rende (CS), Italy
Fax: +39-984-492066
E-mail: d.pucci@unical.it
[b] Centro di Eccellenza CEMIF.CAL, LASCAMM - CR INSTM, Unità INSTM della Calabria and LiCryl, CNR-INFM, Dipartimento di Scienze Farmaceutiche – Università della Calabria, 87036 Arcavacata di Rende (CS), Italy

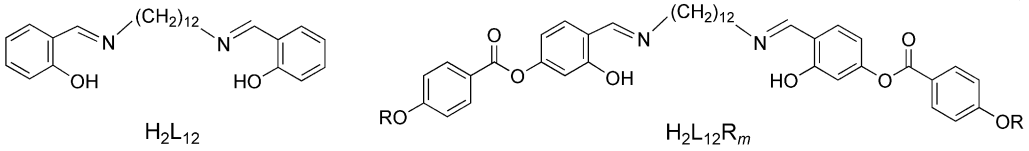

Scheme 1.

or slightly distorted for Cu^{II}) showing the same mesomorphism (nematic or smectic phases) of their precursors, suggesting that an overall rod-like molecular shape is maintained after complexation.[6] However, in order to get the desired luminescence properties not present in the Ni^{II} and Cu^{II} derivatives, we focused on the Zn^{II} ion as coordinating metal able to act as a luminophore centre in such systems. In this paper the synthesis and characterization of a new series of $H_2L_nR_m$ ligands and their corresponding Zn^{II} complexes and the role exerted by the different central spacers (L_n) and terminal chains (R_m) on the overall molecular shape, molecular packing and nature of the potential mesophases in the Zn^{II} derivatives are reported.

Results and Discussion

Synthesis and Characterization

The series of dimeric ligands $H_2L_nR_m$ containing two identical salicylaldimine fragments connected by long even-numbered alkylene spacer were prepared as yellow solids in high yields in a two-step reaction starting from the 2,4-dihydroxybenzaldehyde and the appropriate 4-alkoxybenzoic acid, according to the previously reported procedure used for $H_2L_{12}R_6$ and $H_2L_{12}R_{12}$.[6] Because the overall geometries and the subsequent thermal properties of these types of dimeric liquid crystals are strongly dependent on the ratio between the length of the terminal chains and the spacers,[7,8] L_n and R_m in the present case, for the synthesis of this new series of ligands *N*,*N*′-bis[(4′-alkoxy)benzoyloxybenzylidene]-1,10-diaminodecane $H_2L_{10}R_m$ and *N*,*N*′-bis[(4′-alkoxy)benzoyloxybenzylidene]-1,12-diaminododecane $H_2L_{12}R_m$ terminal chains of comparable length or shorter than the spacer length were selected (Scheme 2).

The reaction of the $H_2L_nR_m$ ligands with an equimolar amount of Zn^{II} acetate dihydrate in ethanol under reflux leads to the formation of the corresponding ZnL_nR_m complexes **1**–**6** in very good yields, whose 1:1 ligand to metal stoichiometry and purity were confirmed by elemental analyses, IR and ^1H NMR spectroscopy (Scheme 3).

In particular, the success of the coordination to the Zn^{II} ion was evidenced, in the IR spectra of **1**–**6**, by the disappearance of the OH signal and by the shift of the CN stretching band to lower wavenumbers with respect to the organic ligand and, in the ^1H NMR spectra, from the lack of OH signals and from the upfield shift of the signal attributable to the iminic hydrogen. Moreover, for complexes **1**–**6**, in the IR spectra two different absorption bands centred

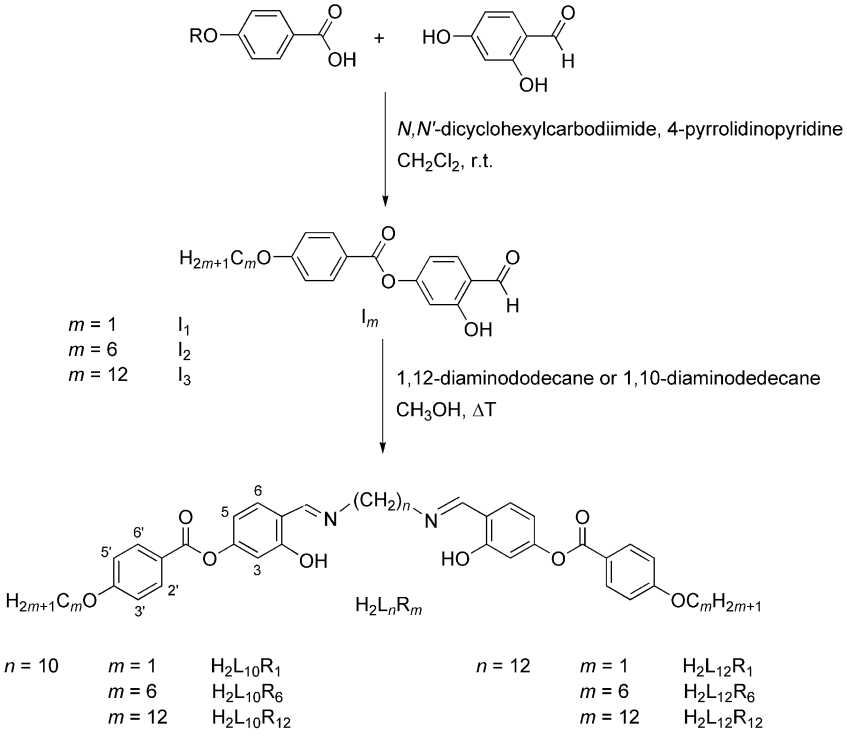

Scheme 2.

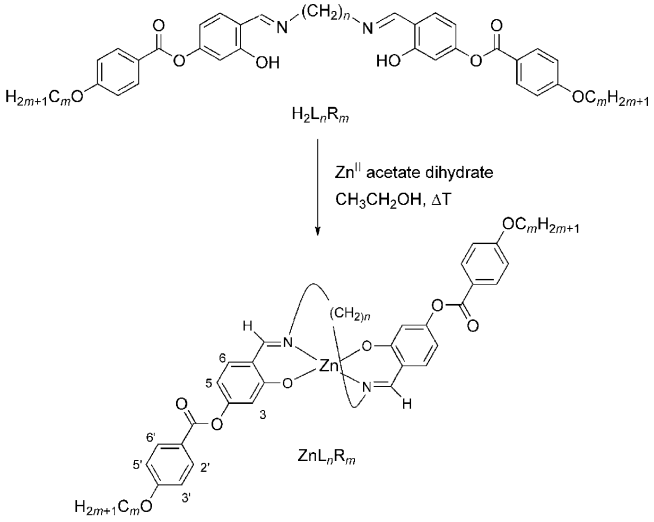

$n = 10$	$m = 1$	$ZnL_{10}R_1$	**1**	$n = 12$	$m = 1$	$ZnL_{12}R_1$	**4**
	$m = 6$	$ZnL_{10}R_6$	**2**		$m = 6$	$ZnL_{12}R_6$	**5**
	$m = 12$	$ZnL_{10}R_{12}$	**3**		$m = 12$	$ZnL_{12}R_{12}$	**6**

Scheme 3.

at about 1530 and 1550 cm^{-1} are observed for the phenolic oxygen atoms and, in the ^1H NMR spectra, two singlets for both the imine groups and the protons in the *ortho* position to the coordinated phenolic oxygen atoms are present, suggesting a loss of symmetry with respect to the starting ligands.

As regards the possible molecular organization and coordination geometry around the zinc(II) centre, in the archetypal Zn(salen) framework the presence of the short central bridge prevents the formation, in the solid state, of a tetrahedral environment, leading to two interchangeable forms: a five-coordinate distorted planar geometry for the monomeric [Zn(salen)L] species[9,10] and a bipyramidal geometry for the $[Zn(salen)]_2$ anhydrous dimeric form.[11] Interestingly, when the alkyl chain between the two imine moieties increases in length ($3 < n < 8$) a greater propensity to form bimetallic or polymeric systems through oxygen-bridging was observed, allowing again the Zn^{II} ion to adopt a five-coordinate environment, but no structural information in the solid state have been reported for Zn^{II} complexes with alkyl backbones longer than three CH_2 groups, suggesting that the structural preferences of the Zn^{II} ion in such Schiff base environments are more complex than thought.[10,12] In the case of complexes **1**–**6**, it appears from all the spectroscopic evidence that the new species show an asymmetric ligand environment around the Zn^{II}, which coupled with the presence of the flexible spacer between the nitrogen donor atoms, direct towards the formation of monomeric derivatives with a distorted tetrahedral geometry. In the absence of experimental structure determination, a model is proposed on the basis of molecular modelling calculations made through the Universal Force Field (UFF) method[13] and performed on complex **3** (Figure 1).

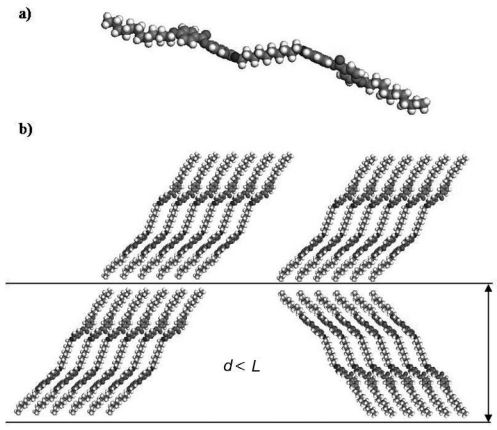

Figure 1. (a) UFF-optimized molecular structure of complex **3** in the fully extended all-*trans* chain conformation and (b) pseudobent core of about 120.4° (chains omitted for clarity).

Thermal Behaviour

All the $H_2L_nR_m$ ligands show, after a crystal-to-crystal transition, mesomorphism typical of calamitic systems, unambiguously recognized by polarized optical microscopy (POM), differential scanning calorimetry (DSC) and temperature-dependent powder X-ray diffraction (PXRD) measurements. Thermal data are summarized in Table 1.

In particular, for the lower homologues the results from POM observations suggested the presence of only a nematic mesophase, as indicated by the typical schlieren ($H_2L_{10}R_1$, $H_2L_{10}R_6$, $H_2L_{12}R_6$) or marbled ($H_2L_{12}R_1$) textures. As regards the ligands with the longest terminal chain R_{12}, $H_2L_{10}R_{12}$ shows only a smectic C phase with an unusual, simultaneous occurrence of schlieren and fun-shaped textures (Figure 2), whereas $H_2L_{12}R_{12}$ exhibited a smectic C phase followed by the nematic one, both identified with a schlieren texture showing only four-brush defects.

All the mesophases are enantiotropically exhibited for several heating/cooling cycles. As expected, the clearing points decreased with the elongation of the terminal chains R_m.

The definitive mesophase identification was achieved by temperature-dependent PXRD analysis on nonaligned samples. The nematic nature of the mesophase was confirmed: in all cases, the diffuse in the small-angle region arises from correlations in the molecular arrangement along the director. In the case of the highest homologues $H_2L_{10}R_{12}$ and $H_2L_{12}R_{12}$, the PXRD patterns revealed the presence of a lamellar smectic phase. In particular, both spectra show three sharp peaks in the low-angle region (46.8, 23.3, 15.7 Å for $H_2L_{10}R_{12}$; 50.4, 25.8, 16.2 Å for $H_2L_{12}R_{12}$) with a reciprocal space ratio of 1:2:3. The maxima can be assigned to the (001), (002) and (003) reflections typical of a layered arrangement. In both cases, the wide angle region displayed a broad halo centred at 4.6–4.7 Å, typical of disordered smectic structures and associated with short-range liquid-like positional order within the layer. The layer thickness *d* of 46.8 and 50.2 Å, deduced from the Bragg spacings of the low-angle reflections, is significantly smaller than the length

Table 1. Thermal behaviour of the $H_2L_nR_m$, ligands.

Compound	Transition[a]	T [°C][b]	ΔH [kJ mol^{-1}]
$H_2L_{10}R_1$	Cr–Cr'	61.2	1.5
	Cr'–N	123.5	31.5
	N–I	157.3	5.5
	I–N	149.6	0.8
	N–C	72.3	0.3
$H_2L_{10}R_6$	Cr–Cr'	61.5	5.8
	Cr'–N	131.3	42.7
	N–I	147.3	6.5
	I–N	146.9	7.0
	N–Cr	71.1	29.9
$H_2L_{10}R_{12}$	Cr–Cr'	82.1	10.6
	Cr'–SmC	98.2	36.7
	SmC–I	133.5	16.7
	I–SmC	133.1	17.0
	SmC–Cr	82.4	39.6
$H_2L_{12}R_1$	Cr–Cr'	125.6	67.4
	Cr'–N	134.6	15.8
	N–I	155.8	7.0
	I–N	154.9	8.1
	N–Cr	73.3	52.0
$H_2L_{12}R_6$	Cr–Cr'	64.7	17.4
	Cr'–N	113.1	43.0
	N–I	133.7	7.7
	I–N	133.1	9.0
	N–Cr	77.8	28.9
$H_2L_{12}R_{12}$	Cr–Cr'	86.9	26.2
	Cr'–SmC	99.6	40.4
	SmC–N	114.8	1.2
	N–I	122.9	8.3
	I–N	122.5	8.4
	N–SmC	114.5	1.6
	SmC–Cr'	77.0	12.3
	Cr'–Cr	74.9	8.6

[a] Cr: Crystal; SmC: smectic C; N: nematic, I: isotropic liquid. [b] Temperature data as onset peak.

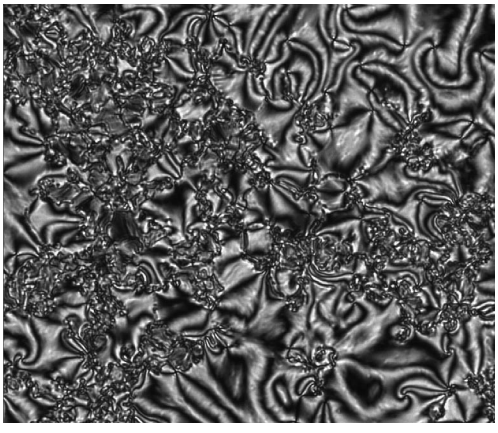

Figure 2. Polarized-light optical photomicrograph of the texture exhibited by $H_2L_{10}R_{12}$ at 130 °C.

L of the molecules, as calculated from the modelled lowest energy conformation of the molecule of $H_2L_{10}R_{12}$ (Figure 3a) of 65 Å. In agreement with the POM observations, the mesophase can be assigned as a tilted smectic C type, with an estimate tilt angle of 43° in the case of $H_2L_{10}R_{12}$, assuming no interdigitation of molecules in adjacent layers (Figure 3b).

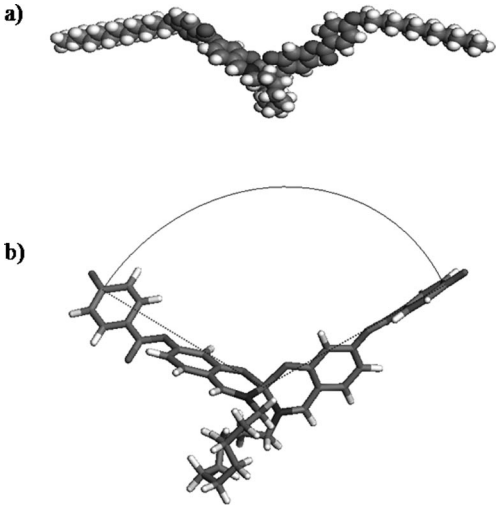

Figure 3. (a) UFF-optimised[13] molecular structure of $H_2L_{10}R_{12}$ in a linear conformation suitable for an overall rod-like shape and (b) schematic representation of the possible arrangements of molecules of $H_2L_{10}R_{12}$ in a tilted layered structure.

Therefore, the presence of nematic and/or smectic C phases in this series of dimeric molecules containing an even number of flexible spacers is an indication of their overall rod molecular geometry, as recently reported in the literature for similar salicylaldimine derivatives.[7]

The thermal behaviour of the ZnL_nR_m complexes (Table 2) was found to be strongly dependent on the ratio between the carbon atom number of the spacer L_n and the terminal chains R_m. Indeed, when $L_n/R_m > 1$ the complexes completely lack mesomorphism, melting directly into an isotropic liquid at very high temperatures, whereas for the higher homologues with $L_n/R_m \leq 1$ a mesophase characterized by a very fine focal conic fan-shaped texture slowly formed from batonnets emerging from the isotropic liquid was observed by POM (Figure 4).

The nature of the mesophase displayed by complexes **3** or **6** was clarified through PXRD measurements performed on nonaligned samples. The PXRD patterns of complexes **3** and **6**, very similar, exhibited sharp inner reflections (22.8, 11.1, 7.3 Å for **3**; 24.8, 11.9, 8.9 Å for **6**) that are consistent with (001), (002), (003) reflections of a layered structure. Furthermore, both spectra showed a diffuse halo centred at 4.6–4.8 Å and associated with the short-range liquid-like positional ordering of the chains. The reduction of the lamellar periodicity d in the zinc complexes with respect to the corresponding ligands evidences a strong interdigitation of the chains as a result of the increase in the molecular area of the core after complexation. Moreover, according to the modelled structure of complex **3**, the coordination of the

Table 2. Thermal behaviour of ZnL_nR_m complexes.

Compound	Transition[a]	T [°C][b]	ΔH [kJ mol^{-1}]
1	Cr–I	312.3[c] (decomp.)	
2	Cr–I	192.9[c]	
3	Cr–$SmC_{intercal}$	183.7	7.2
	$SmC_{intercal}$–I	197.9	18.3
	I–$SmC_{intercal}$	145.0	9.3
	$SmC_{intercal}$–Cr	136.1	0.5
4	Cr–Cr'	128.0[c]	16
	Cr'–I	216.3[c] (decomp.)	
5	Cr–Cr'	68.3	
	Cr'–Cr'	117.2	
		203.6	
	Cr'–I	93.4	
6	Cr–$SmC_{intercal}$	154.9	25.8
	$SmC_{intercal}$–I	169.4	15.1
	I–$SmC_{intercal}$	109.6	36.4

[a] Cr: crystal; Sm: smectic; N: nematic, I: isotropic liquid. [b] Temperature data as onset peak. [c] Data from POM.

Figure 4. Polarized-light optical photomicrograph of the intercalated smectic C phase appearing just below the isotropic phase in complex **6**.

dimeric ligand to the Zn^{II} ion gives rise to an almost regular tetrahedral geometry around the metal ion and an overall pseudobent conformation of the molecule with a reduced length ($L \approx 53$ Å) compared to the free ligand. Therefore, the observed layer spacings d are also less than half of the molecular length of the complex molecules (d/L about 0.4). As a result of the d/L ratio found and the possibility of efficiently packed molecules with strong chain interdigitation between layers, it is possible to propose the formation of an intercalated smectic C phase (Figure 5; designed as B_6 in the case of bent-core structures[14]), often observed for bent-core dimers.[7b,8] Moreover, the quite unusual thermal behaviour including pronounced hysteresis and high viscosity observed for complexes **3** and **6** is in line with the packing of such nonlinear molecules, which induces strong intermolecular dipole–dipole interactions.

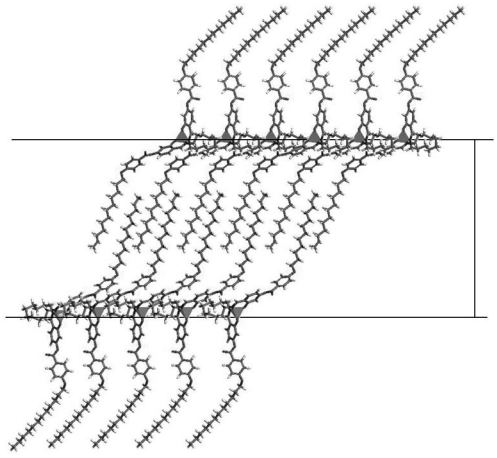

Figure 5. Proposed molecular packing mode in the intercalated smectic C phase.

Photophysical Studies

The photophysical properties of all species were investigated in dichloromethane solution at room temperature. The absorption spectra of the $H_2L_nR_m$ ligands are very similar, showing two peaks centred at 265 and 310 nm and a very-low intensity band at 400 nm. The 265 and 310 nm bands are ascribed to a π–π* transition localized on the aromatic rings, whereas the 400 nm band is due to an n–π* excitation between the lone pair on the iminic nitrogen atom and a π* orbital on the C=N fragment. Complexes **1**–**6** show two intense bands at 275 nm and in the 355–370 nm range resulting from metal-perturbed ligand-centred transitions, which have the same origin as the two principal bands of the ligand spectrum, so proving that Zn^{II} complexation to $H_2L_nR_m$ lowers the energy states of the ligands, leading to a bathochromic shift of the absorption peaks of the complexes. Moreover, as expected, the n–π* transition, which gives rise to a low-intensity band in the $H_2L_nR_m$ spectra, is not detected in the spectra of the corresponding complex because of the involvement of the nitrogen lone pair in the coordination to the Zn^{II} ion.

With reference to the emission properties, whereas the $H_2L_nR_m$ compounds are nonemissive, their corresponding Zn^{II} complexes show the typical large fluorescence band usually observed in similar Schiff-based metal complexes,[4a] with the emission maximum centred at 432 nm originating from π–π* singlet ligand-centred excited state.

Emission quantum yields (EQY) values were determined by using the optically dilute method[15] on aerated dichloromethane solutions whose absorbance at excitation wavelengths was <0.1; 9,10-diphenylanthracene in cyclohexane was used as a standard (EQY = 0.96).[16] The EQY of complexes **1**–**6** are in the 19–22% range and are not significantly affected by the length of the L_n bridge or the R_m substituents.

Emission and excitation spectra of complexes **1**–**6** were also recorded in the solid crystalline state by placing a uniform powder sheet between two quartz plates. The charac-

teristic large fluorescent band of Schiff-based metal complexes was detected in all cases at 452 nm, considerably redshifted with respect to that recorded in solution. The EQY measurements of complexes **1**–**6** were performed by means of an integrating sphere, and a value of about 9% was obtained in all cases. Moreover, for mesomorphic $ZnL_{12}R_{12}$ complex **6**, whose mesophase is frozen, on cooling into a glassy state until room temperature, the emission maximum in this aggregation state was found at 440 nm, with an EQY of about 8%. The emission spectra of **6**, recorded in solution and in the different phases, are summarized in Figure 6 and comparing the different traces it is worthy to note that the maximum emission wavelength with the associated redshift in the excitation spectrum increases on going from the solution to the mesophase and to the microcrystalline powder, so evidencing a trend which can be related to a progressive reinforcement of the intermolecular aromatic interactions. This gives rise to a larger electronic delocalization, resulting in an energy lowering of the electronic states.

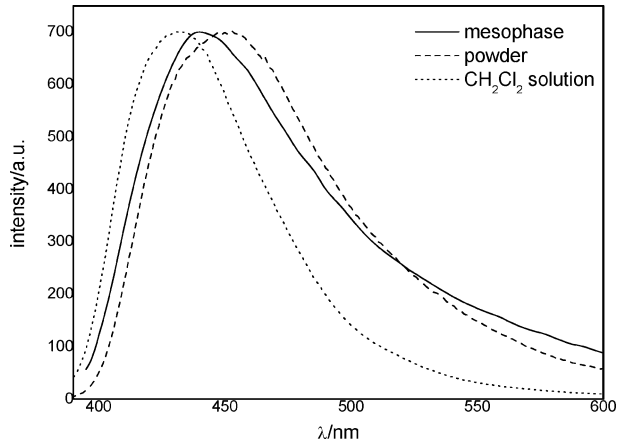

Figure 6. Emission spectra of complex **6**.

In order to comment on the EQY values calculated for **6**, which were found to be 22% in solution, 8% in the mesophase and 9% in the crystalline state, it is reasonable to assume that they could originate from a delicate balance between an enhancement in the intermolecular interactions, which reduces the luminescence intensity (as can be observed on going from the solution to the mesophase), and a reduction in the local mobility, which, on the contrary, favours the radiative deactivation efficiency (as can be observed on going from the mesophase to the crystalline state).

Conclusions

A series of mesogenic tetradentate Schiff bases, $H_2L_nR_m$, containing two identical salicylaldimine fragments (bearing alkoxy substituents of variable length in the 4-position of the terminal aromatic ring) connected through a long, highly flexible even-numbered spacer of variable length was successfully synthesized and characterized. For all these dimeric $H_2L_nR_m$ compounds, according to the global rod-like molecular shape, mesomorphism characteristic of calamitic systems is observed, whose nature is strongly influenced by the ratio between the length of the central bridge L_n and the terminal chains R_m. Indeed, when the R_m length is smaller then the L_n spacer, only a nematic phase is shown, whereas the smectic C is added or replaces the nematic one when the two lengths are comparable.

The addition of Zn^{II} acetate to this series of dimers afforded the corresponding ZnL_nR_m derivatives, for which the intrinsic flexibility of the very long spacer and the presence of the tetrahedral centre induce a bent core geometry favouring, in the homologues with the longest terminal chains, the onset of an intercalated tilted smectic C phase (or B_6 in the banana phases nomenclature), with the molecules intercalated and tilted within the layers. This is a phase normally observed for organic dimers formed by two rod-like segments covalently linked to a central angular aromatic core when the length of the terminal chains is smaller or comparable to the length of the spacer in the dimers. In the present case, it is the metal scaffold that promotes the space-filling interactions, which originate from the bent core structure and which result in the formation of a B phase.

Moreover, the complexation with Zn^{II} turns on, in solution, an intense luminescence in the ZnL_nR_m complexes at 432 nm with a valuable high emission quantum yield of about 20%. This emission, centred on the Zn^{II} salicylaldimine core, is successfully preserved in the mesogenic phase of complex **6**, which emits in the blue spectral range (CIE 1931 chromaticity coordinates $x = 0.2025$, $y = 0.1827$) with a considerable EQY value of 8%.

The described liquid crystalline compounds are interesting blue emitters that combine fluidity and orientational ability so proving that these easy-to-synthesize Zn^{II} complexes can actually form an interesting class of multifunctional materials whose properties are easily modulated through little changes in the single molecular tectons.

Experimental Section

General Methods: Infrared spectra in KBr were recorded with a Perkin–Elmer Spectrum One FTIR spectrometer equipped for reflectance measurements. ^1H NMR spectra were recorded with a Bruker WH-300 spectrometer in $CDCl_3$ solutions, with TMS as an internal standard. Elemental analyses were performed with a Perkin–Elmer 2400 analyzer. The textures of the mesophases were studied with a Zeiss Axioscope polarizing microscope equipped with a Calctec C0 600 heating stage. The transition temperatures and enthalpies were measured with a Perkin–Elmer Pyris 1 Differential Scanning Calorimeter with a heating and cooling rate of 10 °C min^{-1}. The apparatus was calibrated with indium. Two or more heating/cooling cycles were performed on each sample. The X-ray powder diffraction patterns were obtained by using a Bruker AXS General Area Detector Diffraction System (D8 Discover with GADDS) with monochromated Cu-K_α radiation (λ = 1.5406 Å). The highly sensitive area detector was placed at a distance of 20 cm from the sample and at an angle $2\theta_D$ of 14°. A CalCTec (Italy) variable heating stage was used to heat the samples at a rate of

5.0 °C min^{-1} to the appropriate temperature. Measurements were performed by charging samples in Lindemann capillary tubes with inner diameters of 0.5 mm. Steady-state emission spectra were recorded with a HORIBA Jobin–Yvon Fluorolog-3 FL3-211 spectrometer equipped with a 450 W xenon arc lamp, double-grating excitation and single-grating emission monochromators (2.1 nm mm^{-1} dispersion; 1200 grooves mm^{-1}) and a Hamamatsu R928 photomultiplier tube. Emission and excitation spectra were corrected for source intensity (lamp and grating) and emission spectral response (detector and grating) by standard correction curves. The molar extinction coefficients determination was not performed cause a nonoptimal solubilization of the compounds. The emission quantum yields of the pure samples were obtained by means of a 102 mm diameter integrating sphere coated with Spectralon® and mounted in the optical path of the spectrofluorimeter by using, as excitation source, a 450 W Xenon lamp coupled with a double-grating monochromator for selecting wavelengths. The experimental uncertainties were 1 nm for the band maxima for the luminescence spectra, 10% for EQY in solution and 5% for EQY in pure samples.

Synthesis of the Ligands: The preparation of $I_{2,3}$ precursors and $H_2L_{12}R_6$ and $H_2L_{12}R_{12}$ ligands was accomplished as previously reported.[7] The synthesis of I_1 and other $H_2L_nR_m$ compounds was performed by following the same method.

4-Formyl-3-hydroxyphenyl 4-Methoxybenzoate (I_1): White solid. Yield: 0.86 g (69%). M.p. 117 °C. IR (KBr): $\tilde{\nu}$ = 2951–2846 (stretching aliphatic CH), 1735 (ester stretching C=O), 1658 (aldehydic stretching C=O), 1606, 1254 cm^{-1}. ^{1}H NMR (300 MHz, $CDCl_3$, 25 °C): δ = 11.26 (s, 1 H, OH), 9.89 (s, 1 H, CH=O), 8.13 (d, J = 9.04 Hz, 2 H, H$^{2',6'}$), 7.61 (d, J = 9.04 Hz, 1 H, H^6), 6.99 (d, J = 9.04 Hz, 2 H, H$^{3',5'}$), 6.93 (dd, J = 2.44 Hz, J = 8.54 Hz, 1 H, H^5), 6.87 (d, J = 2.44 Hz, 1 H, H^3), 3.90 (s, 3 H, OCH_3) ppm. $C_{15}H_{12}O_5$ (272.25): calcd. C 66.17, H 4.44; found C 65.81, H 4.16.

***N*,*N*′-Bis[(4′-methoxy)benzoyloxybenzylidene]-1,10-diaminodecane ($H_2L_{10}R_1$):** 1,10-Diaminodecane (0.08 g, 0.46 mmol) was added to a hot solution of I_1 (0.25 g, 0.92 mmol) in methanol (15 mL). The precipitate, which immediately formed, was stirred under reflux for 4 h, then filtered and washed with ethanol. The crude product was purified by recrystallization from acetone and then dried in vacuo. Yellow solid. Yield: 0.25 g (80%). IR (KBr): $\tilde{\nu}$ = 2921–2850 (stretching aliphatic CH), 1728 (stretching C=O), 1635 (stretching C=N), 1606, 1254 cm^{-1}. ^{1}H NMR (300 MHz, $CDCl_3$, 25 °C): δ = 14.11 (s, 2 H, OH), 8.31 (s, 2 H, CH=N), 8.14 (d, J = 8.95 Hz, 4 H, H$^{2',6'}$), 7.26 (d, J = 8.67 Hz, 2 H, H^6), 6.99 (d, J = 8.95 Hz, 4 H, H$^{3',5'}$), 6.79 (d, J = 2.31 Hz, 2 H, H^3), 6.72 (d, J = 2.31, J = 8.67 Hz, 2 H, H^5), 3.89 (s, 6 H, OCH_3), 3.59 (t, J = 7.51 Hz, 4 H, C=N-CH_2), 1.72–1.30 (m, 16 H, aliphatic protons) ppm. UV/Vis (CH_2Cl_2): $\lambda_{abs.}$ = 400, 310, 265 nm. $C_{40}H_{44}N_2O_8$ (680.31): calcd. C 70.57, H 6.51, N 4.11; found C 70.71, H 6.18, N 4.14.

***N*,*N*′-Bis[(4′-hexyloxy)benzoyloxybenzylidene]-1,10-diaminodecane ($H_2L_{10}R_6$):** Yellow solid. Yield: 0.28 g (82%). IR (KBr): $\tilde{\nu}$ = 2925–2846 (stretching aliphatic CH), 1728 (stretching C=O), 1635 (stretching C=N), 1608, 1255 cm^{-1}. ^{1}H NMR (300 MHz, $CDCl_3$, 25 °C): δ = 14.12 (s, 2 H, OH), 8.31 (s, 2 H, CH=N), 8.12 (d, J = 8.52 Hz, 4 H, H$^{2',6'}$), 7.26 (d, J = 8.52 Hz, 2 H, H^6), 6.96 (d, J = 8.83 Hz, 4 H, H$^{3',5'}$), 6.79 (d, J = 2.18 Hz, 2 H, H^3), 6.71 (dd, J = 2.18 Hz, J = 8.20 Hz, 2 H, H^5), 4.04 (t, J = 6.62 Hz, 4 H, OCH_2), 3.58 (t, J = 6.62 Hz, 4 H, C=N-CH_2), 1.86–0.89 (m, 38 H, aliphatic protons) ppm. UV/Vis (CH_2Cl_2): $\lambda_{abs.}$ = 400, 310, 265 nm. $C_{50}H_{64}N_2O_8$ (821.05): calcd. C 73.14, H 7.86, N 3.41; found C 72.98, H 8.01, N 3.32.

***N*,*N*′-Bis[(4′-dodecyloxy)benzoyloxybenzylidene]-1,10-diaminodecane ($H_2L_{10}R_{12}$):** Yellow solid. Yield: 0.32 g (79%). IR (KBr): $\tilde{\nu}$ = 2920–2849 (stretching aliphatic CH), 1728 (stretching C=O), 1640 (stretching C=N), 1606, 1254 cm^{-1}. ^{1}H NMR (300 MHz, $CDCl_3$, 25 °C): δ = 14.10 (s, 2 H, OH), 8.31 (s, 2 H, CH=N), 8.13 (d, J = 8.80 Hz, 4 H, H$^{2',6'}$), 7.26 (d, J = 8.27 Hz, 2 H, H^6), 6.97 (d, J = 8.80 Hz, 4 H, H$^{3',5'}$), 6.79 (d, J = 1.87 Hz, 2 H, H^3), 6.72 (dd, $J_{3,5}$ = 1.87 Hz, J = 8.54 Hz, 2 H, H^5), 4.04 (t, J = 6.95 Hz, 4 H, OCH_2), 3.58 (t, J = 6.90 Hz, 4 H, C=N-CH_2), 1.86–0.90 (m, 62 H, aliphatic protons) ppm. UV/Vis (CH_2Cl_2): $\lambda_{abs.}$ = 400, 310, 265 nm. $C_{62}H_{88}N_2O_8$ (989.37): calcd. C 75.27, H 8.97, N 2.83; found C 75.33, H 8.88, N 3.16.

***N*,*N*′-Bis[(4′-methoxy)benzoyloxybenzylidene]-1,12-diaminododecane ($H_2L_{12}R_1$):** Yellow solid. Yield: 0.29 g (77%). IR (KBr): $\tilde{\nu}$ = 2927–2853 (stretching aliphatic CH), 1731 (stretching C=O), 1637 (stretching C=N), 1606, 1256 cm^{-1}. ^{1}H NMR (300 MHz, $CDCl_3$, 25 °C): δ = 14.12 (s, 2 H, OH), 8.32 (s, 2 H, CH=N), 8.14 (d, J = 8.79 Hz, 4 H, H$^{2',6'}$), 7.26 (d, J = 8.47 Hz, 2 H, H^6), 6.98 (d, J = 8.79 Hz, 4 H, H$^{3',5'}$), 6.78 (d, J = 2.48 Hz, 2 H, H^3), 6.72 (d, $J_{3,5}$ = 2.48 Hz, J = 8.47 Hz, 2 H, H^5), 3.90 (s, 6 H, OCH_3), 3.58 (t, J = 7.38 Hz, 4 H, C=N-CH_2), 1.71–1.28 (m, 20 H, aliphatic protons) ppm. UV/Vis (CH_2Cl_2): $\lambda_{abs.}$ = 400, 310, 265 nm. $C_{42}H_{48}N_2O_8$ (708.34): calcd. C 71.17, H 6.83, N 3.95; found C 71.49, H 6.71, N 3.64.

$ZnL_{10}R_1$ (1): Zinc acetate dihydrate (0.05 g, 0.02 mmol) was added to a hot solution of HL_1 (0.15 g, 0.21 mmol) in ethanol (15 mL). The reaction mixture was stirred at reflux for 5 h and then cooled to room temperature. The solid, collected by filtration, was purified by recrystallization from chloroform/acetonitrile and then dried in vacuo. White solid. Yield: 0.14 g (89%). IR (KBr): $\tilde{\nu}$ = 2932–2856 (stretching aliphatic CH), 1725 (stretching C=O), 1605 (stretching C=N), 1255 cm^{-1}. ^{1}H NMR (300 MHz, $CDCl_3$, 25 °C): δ = 8.18 (s, 2 H, CH=N), 8.14 (d, J = 8.83 Hz, 4 H, H$^{2',6'}$), 7.15 (t, J = 8.51 Hz, 2 H, H^6), 6.98 (d, J = 8.83 Hz, 4 H, H$^{3',5'}$), 6.65 (d, J = 1.89 Hz, 2 H, H^3), 6.51 (dd, J = 1.89 Hz, J = 8.51 Hz, 2 H, H^5), 4.05 (s, 6 H, OCH_3), 4.15, 3.82 (m, 4 H, C=N-CH_2), 1.34-1.16 (m, 16 H, aliphatic protons) ppm. UV/Vis (CH_2Cl_2): $\lambda_{abs.}$ = 370, 275 nm; $\lambda_{em.}$ = 432 nm. $C_{40}H_{42}N_2O_8Zn$ (744.16): calcd. C 64.56, H 5.69, N 3.76; found C 64.78, H 5.52, N 3.89.

$ZnL_{10}R_6$ (2): White solid. Yield: 0.16 g (85%). IR (KBr): $\tilde{\nu}$ = 2924–2848 (stretching aliphatic CH), 1730 (stretching C=O), 1606 (stretching C=N), 1267 cm^{-1}. ^{1}H NMR (300 MHz, $CDCl_3$, 25 °C): δ = 8.17 (s, 2 H, CH=N), 8.12 (d, J = 8.86 Hz, 4 H, H$^{2',6'}$), 7.14 (t, J = 8.60 Hz, 2 H, H^6), 6.95 (d, J = 8.86 Hz, 4 H, H$^{3',5'}$), 6.65 (d, J = 1.89 Hz, 2 H, H^3), 6.51 (dd, J = 1.89 Hz, J = 8.33 Hz, 2 H, H^5), 4.04 (t, J = 6.45 Hz, 4 H, OCH_2), 3.83, 3.32 (m, 4 H, C=NCH_2), 1.86–0.89 (m, 38 H, aliphatic protons) ppm. UV/Vis (CH_2Cl_2): $\lambda_{abs.}$ = 355, 275 nm; $\lambda_{em.}$ = 432 nm. $C_{50}H_{62}N_2O_8Zn$ (884.43): calcd. C 67.90, H 7.07, N 3.17; found C 67.58, H 7.25, N 2.92. Thermal behaviour is reported in Table 2.

$ZnL_{10}R_{12}$ (3): White solid. Yield: 0.11 g (82%). IR (KBr): $\tilde{\nu}$ = 2946–2853 (stretching aliphatic CH), 1732 (stretching C=O), 1605 (stretching C=N), 1254 cm^{-1}. ^{1}H NMR (300 MHz, $CDCl_3$, 25 °C): δ = 8.17 (s, 2 H, CH=N), 8.12 (d, J = 8.84 Hz, 4 H, H$^{2',6'}$), 7.13 (t, J = 8.55 Hz, 2 H, H^6), 6.95 (d, J = 8.84 Hz, 4 H, H$^{3',5'}$), 6.64 (d, J = 2.49 Hz, 2 H, H^3), 6.51 (dd, J = 2.49 Hz, J = 8.55 Hz, 2 H, H^5), 4.03 (t, J = 6.36 Hz, 4 H, OCH_2), 3.83, 3.33 (m, 4 H, C=N-CH_2), 1.83–0.86 (m, 62 H, aliphatic protons) ppm. UV/Vis (CH_2Cl_2): $\lambda_{abs.}$ = 360, 275 nm; $\lambda_{em.}$ = 432 nm. $C_{62}H_{86}N_2O_8Zn$ (1052.74): calcd. C 70.74, H 8.23, N 2.66; found C 70.88, H 8.15, N 2.49. Thermal behaviour is reported in Table 2.

$ZnL_{12}R_1$ (4): White solid. Yield: 0.13 g (75%). IR (KBr): $\tilde{\nu}$ = 2931–2855 (stretching aliphatic CH), 1735 (stretching C=O), 1607 (stretching C=N), 1258 cm^{-1}. ^1H NMR (300 MHz, $CDCl_3$, 25 °C): δ = 8.18 (s, 2 H, CH=N), 8.13 (d, J = 8.79 Hz, 4 H, $H^{2',6'}$), 7.13 (t, J = 8.79 Hz, 2 H, H^6), 6.97 (d, J = 8.82 Hz, 4 H, $H^{3',5'}$), 6.64 (d, J = 2.19 Hz, 2 H, H^3), 6.48 (dd, J = 2.19 Hz, J = 8.79 Hz, 2 H, H^5), 3.90 (s, 6 H, OCH_3), 3.83, 3.32 (m, 4 H, C=N-CH_2), 1.28–0.95 (m, 20 H, aliphatic protons) ppm. UV/Vis (CH_2Cl_2): $\lambda_{abs.}$ = 360, 275 nm; $\lambda_{em.}$ = 432 nm. $C_{42}H_{46}N_2O_8Zn$ (772.21): calcd. C 65.33, H 6.00, N 3.63; found C 65.18, H 6.15, N 3.89. Thermal behaviour is reported in Table 2.

$ZnL_{12}R_6$ (5): White solid. Yield: 0.13 g (80%). IR (KBr): $\tilde{\nu}$ = 2926–2854 (stretching aliphatic CH), 1732 (stretching C=O), 1606 (stretching C=N), 1535, 1255 cm^{-1}. ^1H NMR (300 MHz, $CDCl_3$, 25 °C): δ = 8.17 (s, 2 H, CH=N), 8.11 (d, J = 8.54 Hz, 4 H, $H^{2',6'}$), 7.14 (t, J = 8.54 Hz, 2 H, H^6), 6.95 (d, J = 8.54 Hz, 4 H, $H^{3',5'}$), 6.65 (d, J = 2.44 Hz, 2 H, H^3), 6.51 (dd, J = 2.44 Hz, J = 8.54 Hz, 2 H, H^5), 4.04 (t, J = 6.10 Hz, 4 H, OCH_2), 3.81, 3.33 (m, 4 H, C=NCH_2), 1.87–0.88 (m, 42 H, aliphatic protons) ppm. UV/Vis (CH_2Cl_2): $\lambda_{abs.}$ = 360, 275 nm; $\lambda_{em.}$ = 432 nm. $C_{52}H_{66}N_2O_8Zn$ (912.48): calcd. C 68.45, H 7.29, N 3.07; found C 68.28, H 7.25, N 2.89. Thermal behaviour is reported in Table 2.

$ZnL_{12}R_{12}$ (6): White solid. Yield: 0.12 g (76%). IR (KBr): $\tilde{\nu}$ = 2924–2853 (stretching aliphatic CH), 1732 (stretching C=O), 1606 (stretching C=N), 1535, 1254 cm^{-1}. ^1H NMR (300 MHz, $CDCl_3$, 25 °C): δ = 8.17 (s, 2 H, CH=N), 8.11 (d, J = 8.54 Hz, 4 H, $H^{2',6'}$), 7.14 (t, J = 8.54 Hz, 2 H, H^6), 6.95 (d, J = 8.54 Hz, 4 H, $H^{3',5'}$), 6.65 (d, J = 2.44 Hz, 2 H, H^3), 6.50 (dd, J = 2.44 Hz, J = 8.54 Hz, 2 H, H^5), 4.03 (t, J = 6.10 Hz, 4 H, OCH_2), 3.79, 3.31 (m, 4 H, C=N-CH_2), 1.85–0.83 (m, 66 H, aliphatic protons) ppm. UV/Vis (CH_2Cl_2): $\lambda_{abs.}$ = 355, 275 nm; $\lambda_{em.}$ = 432 nm. $C_{64}H_{90}N_2O_8Zn$ (1080.80): calcd. C 71.12, H 8.39, N 2.59; found C 71.28, H 8.45, N 2.28. Thermal behaviour is reported in Table 2.

Acknowledgments

Financial support received from the Ministero dell'Istruzione, dell'Università e della Ricerca Scientifica (MIUR) through the Centro di Eccellenza CEMIF.CAL (CLAB01TYEF) and the PRIN projects 2006038447 and 2007WJMF2W is gratefully acknowledged.

[1] a) T. Sano, Y. Nishio, Y. Hamada, H. Takahashi, T. Usuki, K. Shibata, *J. Mater. Chem.* **2000**, *10*, 157–161; b) R. C. Evans, P. Douglas, C. J. Winscom, *Coord. Chem. Rev.* **2006**, *250*, 2093–2126; c) X. Xu, Y. Liao, G. Yu, H. You, C. Di, Z. Su, D. Ma, Q. Wang, S. Li, S. Wang, J. Ye, Y. Liu, *Chem. Mater.* **2007**, *19*, 1740–1748; d) H.-J. Son, W.-S. Han, J.-Y. Chun, B.-K. Kang, S.-N. Kwon, J. Ko, S. J. Han, C. Lee, S. J. Kim, S. O. Kang, *Inorg. Chem.* **2008**, *47*, 5666–5676; e) P. D. Vellis, J. A. Mikroyannidis, C.-N. Lo, C.-S. Hsu, *J. Polym. Sci., Part A: Polym. Chem.* **2008**, *46*, 7702–7712; f) V. K. Rai, R. Srivastava, G. Chauhan, K. Saxena, R. K. Bhardwaj, S. Chand, M. N. Kamalasanan, *Mater. Lett.* **2008**, *62*, 2561–2563; g) L. Chen, J. Qiao, J. Xie, L. Duan, D. Zhang, L. Wang, Y. Qiu, *Inorg. Chim. Acta* **2009**, *362*, 2327–2333.

[2] a) M. O'Neill, S. M. Kelly, *Adv. Mater.* **2003**, *15*, 1135–1146; b) J. Hanna, *Opto-Electron. Rev.* **2005**, *13*, 259–267; c) S. Laschat, A. Baro, N. Steinke, F. Giesselmann, C. Hoegele, G. Scalia, R. Judele, E. Kapatsina, S. Sauer, A. Schreivogel, M. Tosoni, *Angew. Chem. Int. Ed.* **2007**, *46*, 4832–4887; d) F. Camerel, J. Barberá, J. Otsuki, T. Tokimoto, Y. Shimazaki, L.-Y. Chen, S.-H. Liu, M.-S. Lin, C.-C. Wu, R. Ziessel, *Adv. Mater.* **2008**, *20*, 3462–3467; e) T. Yasuda, H. Ooi, J. Morita, Y. Akama, K. Minoura, M. Funahashi, T. Shimomura, T. Kato, *Adv. Funct. Mater.* **2009**, *19*, 411–419.

[3] a) E. Terrazzi, J.-m. Bénech, J.-P. Rivera, G. Bernardinelli, B. Donnio, D. Guillon, C. Piguet, *Dalton Trans.* **2003**, 769–772; b) F. Morale, R. W. Date, D. Guillon, D. W. Bruce, R. L. Finn, C. Wilson, A. J. Blake, M. Schöder, B. Donnio, *Chem. Eur. J.* **2003**, *9*, 2484–2501; c) R. Giménez, A. B. Manrique, S. Uriel, J. Barberá, J. L. Serrano, *Chem. Commun.* **2004**, 2064–2064; d) G. Barberio, A. Bellusci, A. Crispini, M. Ghedini, A. Golemme, P. Prus, D. Pucci, *Eur. J. Inorg. Chem.* **2005**, 181–188; e) E. Cavero, S. Uriel, P. Romero, J. L. Serrano, R. Giménez, *J. Am. Chem. Soc.* **2007**, *129*, 11608–11618; f) I. Aiello, A. Bellusci, A. Crispini, M. Ghedini, D. Pucci, T. Spataro, *Mol. Cryst. Liq. Cryst.* **2008**, *481*, 1–13; g) P. Ovejero, M. J. Mayoral, M. Cano, J. A. Campo, J. V. Heras, P. Fernández-Tobar, M. Valién, E. Pinilla, M. R. Torres, *Mol. Cryst. Liq. Cryst.* **2008**, *481*, 34–55; h) K. A. Ames, S. R. Collinson, A. J. Blake, C. Wilson, J. B. Love, D. W. Bruce, B. Donnio, D. Guillon, M. Schröder, *Eur. J. Inorg. Chem.* **2008**, 5056–5066; i) F. Morale, R. L. Finn, S. R. Collinson, A. J. Blake, C. Wilson, D. W. Bruce, D. Guillon, B. Donnio, M. Schroöder, *New J. Chem.* **2008**, *32*, 297–305.

[4] a) P. G. Cozzi, L. S. Dolci, A. Garelli, M. Montalti, L. Prodi, N. Zaccheroni, *New J. Chem.* **2003**, *27*, 692–697; b) T. Yu, W. Su, W. Li, Z. Hong, R. Hua, B. Li, *Thin Solid Films* **2007**, *515*, 4080–4084; c) S. J. Wezenberg, A. W. Kleij, *Angew. Chem. Int. Ed.* **2008**, *47*, 2354–2364.

[5] M. La Deda, M. Ghedini, I. Aiello, A. Grisolia, *Chem. Lett.* **2004**, *33*, 1060–1061.

[6] D. Pucci, I. Aiello, A. Bellusci, G. Callipari, A. Crispini, M. Ghedini, *Mol. Cryst. Liq. Cryst.* **2009**, *500*, 144–154.

[7] a) M. Sêpelj, A. Lesac, U. Baumeister, S. Diele, D. W. Bruce, Z. Hameršak, *Chem. Mater.* **2006**, *18*, 2050–2058; b) M. Sêpelj, A. Lesac, U. Baumeister, S. Diele, H. L. Nguyen, D. W. Bruce, *J. Mater. Chem.* **2007**, *17*, 1154–1165.

[8] a) . T. Imrie, P. A. Henderson, *Chem. Soc. Rev.* **2007**, *36*, 2096–2124; b) C. V. Yelamaggad, S. A. Nagamani, U. S. Hiremath, D. S. S. Rao, S. K. Prasad, *Liq. Cryst.* **2002**, *29*, 1401–1408; c) R. Achten, A. Koudijs, Z. Karczamarzyk, A. T. M. Marcelis, E. J. R. Sudholter, *Liq. Cryst.* **2004**, *31*, 215–227.

[9] D. Hall, F. H. Moore, *J. Chem. Soc. A* **1966**, 1822–1824.

[10] J. Reglinski, S. Morris, D. E. Stevenson, *Polyhedron* **2002**, *21*, 2175–2182.

[11] G. E. Batley, D. P. Graddon, *Aust. J. Chem.* **1967**, *20*, 885–891.

[12] J. Sanmartín Matalobos, A. M. García-Deibe, M. Fondo, D. Navarro, M. R. Bermejo, *Inorg. Chem. Commun.* **2004**, *7*, 311–314.

[13] Molecular modelling was performed by using the UFF force field (A. K. Rappè, C. Casewit, K. S. Colwell, W. A. Goddard III, W. M. Skiff, *J. Am. Chem. Soc.* **1992**, *114*, 10024–10035) implemented in the software package *Program Cerius3.0* (Molecular Simulation Inc., **1997**).

[14] a) G. Pelz, S. Diele, W. Weissflog, *Adv. Mater.* **1999**, *11*, 707–724; b) R. A. Reddy, C. Tschierske, *J. Mater. Chem.* **2006**, *16*, 907–961.

[15] J. N. Demas, G. A. Crosby, *J. Phys. Chem.* **1971**, *75*, 991–1024.

[16] W. R. Ware, W. Rothman, *Chem. Phys. Lett.* **1976**, *39*, 449–453.

Received: June 15, 2009
Published Online: August 31, 2009

